Eur. Phys. J. B **33**, 193–202 (2003)
DOI: 10.1140/epjb/e2003-00156-9

THE EUROPEAN PHYSICAL JOURNAL B

Determination of the stochastic evolution equation from noisy experimental data

J. Maunuksela[1,a], M. Myllys[1], J. Merikoski[1], J. Timonen[1], T. Kärkkäinen[2], M.S. Welling[3], and R.J. Wijngaarden[3]

[1] Department of Physics, PO Box 35 (YFL), 40014 University of Jyväskylä, Finland
[2] Department of Mathematical Information Technology, PO Box 35 (Agora), 40014 University of Jyväskylä, Finland
[3] Faculty of Science, Vrije Universiteit, De Boelelaan 1081, 1081 HV Amsterdam, The Netherlands

Received 20 December 2002 / Received in final form 7 March 2003
Published online 4 June 2003 –

Abstract. We have determined the coefficients of the Kardar-Parisi-Zhang equation as functions of coarse graining, which best describe the time evolution and spatial behavior observed for slow-combustion fronts in sheets of paper and magnetic flux fronts in a thin-film high-T_c superconductor. Reconstruction of the relevant equation of motion and its coefficients was mainly based on the inverse method proposed by Lam and Sander [Phys. Rev. Lett. **71**, 561 (1993)]. The coefficient of the nonlinear term was also determined from the local slope-dependence of the front velocity.

PACS. 05.10.Gg Stochastic analysis methods (Fokker-Planck, Langevin, etc.) – 05.40.-a Fluctuation phenomena, random processes, noise, and Brownian motion – 64.60.Ht Dynamic critical phenomena

1 Introduction

The phenomena of kinetic roughening [1–4] of driven interfaces are abundant in Nature. They can be observed in the propagation of a forest fire or in the spreading of a coffee stain in a paper towel. Both examples display, under suitable conditions, a distinct *interface* moving through a *random* medium, which becomes rough as time evolves. From an experimental point of view convenient systems for studying this kind of kinetic roughening phenomena include slow-combustion (smouldering) fronts propagating in sheets of paper [5–8] and magnetic flux fronts penetrating thin-film high-T_c superconductors [9].

A classification of kinetic roughening phenomena can be obtained by relating the observed dynamics to those of an appropriate Langevin equation with a noise term which may have system specific correlations and even a non-Gaussian magnitude distribution [3,4]. It has been shown that the large-scale dynamics of a wide class of roughening phenomena can be modelled with that kind of continuum *stochastic partial differential equations*, such as the Kardar-Parisi-Zhang (KPZ) equation [10] and its variations [3,4]. For a moving interface the KPZ equation is usually expressed in the form

$$\partial_t h = c + \nu\nabla^2 h + \frac{\lambda}{2}(\nabla h)^2 + \eta \,, \qquad (1)$$

where $h \equiv h(x,t)$ is the height of the interface, c its zero-slope velocity, and η denotes the effective noise. If η is short-range correlated in time and space, it can be asymptotically substituted by uncorrelated Gaussian (white) noise: $\langle\eta(x,t)\rangle = 0$ and $\langle\eta(x,t)\eta(x',t')\rangle = 2D\delta(x-x')$ $\times\delta(t-t')$.

Different approaches can be taken to determine the possible universality class, with an appropriate evolution equation, which the considered process belongs to. A straightforward and much used method is to measure some of its scaling properties, such as (typically) a scaling exponent, and compare them (it) with the ones obtained analytically or numerically for known models. The asymptotic scaling properties on long length and time scales of the smouldering fronts, as well as of the magnetic flux fronts, were shown in this way to be well described by equation (1) with uncorrelated white noise [6,8,9]. Another approach, which however has not been used on experimental data before, is to directly determine the evolution equation from simulated or observed front evolution.

Several methods have been proposed for realizing the latter approach, *i.e.*, for the determination of the terms and their coefficients in a growth equation that provide the best fit to a known set of time-dependent and spatially varying fronts. The variation of the growth velocity with surface inclination has also been used by several authors to classify the scaling properties of different systems [11–13]. Albert *et al.* [14] showed that the universality class can thus be determined from snapshots of the interface profile, and analyzed in this way interfaces obtained from fluid-flow experiments. Lam and Sander [15] showed that the relevant terms and their coefficients can be determined

[a] e-mail: jussi.maunuksela@physmail.phys.jyu.fi

from simulated interfaces using an inverse method. They proposed that the method may also be used on experimental data. Giacometti and Rossi [16] suggested that the model parameters can be extracted using an approach based on the Fokker-Planck equation combined with a least-squares error procedure. They later reported [17] that the parameters of the KPZ equation should be able to be determined reliably using an improved scheme that hinges on a spectral representation of the KPZ equation.

While results are thus available on the extraction of the terms and their coefficients for equations that describe simulated interfaces, very little has been done on real observed interfaces. In this article we now report results for the terms and their coefficients in a stochastic partial differential equation which best describes the front evolution observed in smouldering fronts and magnetic flux fronts.

2 Experiments and data

The main components of the experimental system used for smouldering fronts included a combustion chamber, a camera system, and a computer with necessary hardware and software. Experiments were initiated by igniting a sheet of paper with an electrical heating wire stretched across the paper sample. The propagation of the emerging one-dimensional fronts was recorded with a three-CCD-camera system including a fast on-line compression of images for increased spatial and temporal resolution Δx and Δt, respectively. A detailed description of the experimental setup and the preparation of the samples can be found in reference [8].

The sample used for the magnetic flux penetration experiment was a $YBa_2Cu_3O_{7-x}$(YBCO) thin (80 nm) film on $NdGaO_3$ substrate. The thin film was patterned, using standard photolithography, in stripes with an aspect ratio of 1:9 in the a-b plane, the long edge having a length of 8.1 mm. The flux penetration was visualized using an advanced magneto-optic image lock-in amplifier [18], by which we directly determined the perpendicular component of the magnetic field H_z at the surface of the sample. The advantage of this technique, compared to conventional magneto-optics, is the improved sensitivity at small magnetic fields, the intrinsic linearity in field, and the direct measurement of the sign of the field. The sample was cooled in zero field to 4.2 K. After temperature stabilization the magnetic field was applied perpendicular to the sample surface, and stepwise increased from zero to 17 mT. In every step the field was increased by 50 mT with a sweeprate of 1 mT/s. After each step and a time-delay of 6 seconds, the image was recorded. Images were recorded with a charge-coupled device (CCD) camera using an acquisition time of 750 ms. Only the middle part of the long edges of the sample was used for analysis to eliminate the effects of the corners on the shape of the fronts. The flux front was determined from the MO image as the borderline between the Shubnikov region, where vortices are present, and the flux-free (Meissner) region. At this borderline, by definition, the local intensity equals the intensity of the Meissner region plus 3 times the standard deviation of the noise in this intensity. Magnification was such that a pixel corresponded to 1.4 μm.

The effective coefficients applicable in equation (1) were estimated for smouldering fronts $h(x,t)$ of width L, as terms of higher order were found to be irrelevant (see below for a discussion on this). The front data used here include those of (i) 18 burns of Kangas copier-paper and (ii) 32 burns of Whatman lens-paper sheets. The sample width L was approximately 28 cm ($\Delta x = 273.4$ μm, $\Delta t = 0.4$ s) and 14 cm ($\Delta x = 137.6$ μm, $\Delta t = 0.1$ s) for copier- and lens-paper samples, respectively. The magnetic flux fronts were affected by some macroscopic defects in the sample used, which limited the width of the analyzed stripe to 358 μm ($\Delta x = 1.4$ μm, $\Delta t = 50$ ms). In the lens-paper and flux-front data, digitizing errors and other erratic non-Gaussian factors in the recorded fronts were reduced by using a new filtering method (see Appendix A).

3 Inverse method

3.1 Description of the method

The inverse method applied here closely follows the general approach proposed by Lam and Sander [15]: the evolution equation for the fronts is first written in the form

$$\frac{\partial h(x,t)}{\partial t} = \mathbf{a}\cdot\mathbf{H}(x,t) + \eta(x,t), \tag{2}$$

where $\mathbf{a}$ is a vector that contains the relevant coefficients of the equation, *e.g.*, $\mathbf{a} = (\nu, \lambda/2, \dots)$, and $\mathbf{H}(x,t)$ is a vector containing derivatives of $h(x,t)$ and powers of these derivatives. Since the observed quantities are determined from the experimental data composed of digital front images, the single-valued function $h(x,t)$ is replaced by $h_i(t)$ with subscript i the lattice index. The lattice has spacing Δx and $N \equiv L/\Delta x$ sites, where L is the sample width. The time interval between subsequent images is denoted by Δt. One then discretizes equation (2) so that it is coarse grained up to length ℓ and up to time τ (a multiple of Δt), such that

$$\frac{\Delta h_i(t)}{\tau} \simeq \mathbf{a}\cdot\mathbf{H}_i(t) + \eta_i(t). \tag{3}$$

For the KPZ equation, equation (1), the parameter vector $\mathbf{a}$ and the interface derivative vector $\mathbf{H}$, respectively, are of the form

$$\mathbf{a} = \left[c, \nu, \frac{\lambda}{2}\right], \tag{4}$$

$$\mathbf{H}_i(t) = \left[1, \nabla^2 h, (\nabla h)^2\right]. \tag{5}$$

In this work $\mathbf{a}$ and $\mathbf{H}$ were mainly of this form, but also higher-order derivatives were tested in $\mathbf{H}$, and corresponding additional coefficients in $\mathbf{a}$. Since the average height of the fronts $\overline{h}(t) = (1/N)\sum_i h_i(t)$ had in all cases a clear linear trend in time, the zero-slope velocity c was assumed to be constant. To determine $\mathbf{H}_i(t)$, all the fronts were

first coarse grained by truncating their Fourier components with wavelengths smaller than ℓ. This means that from the (discrete) Fourier transforms of the front heights,

$$\hat{h}_{q_n}(t) = \Delta x \sum_{i=1}^{N} \mathrm{e}^{-\mathrm{i}q_n x_i}\ h_i(t), \tag{6}$$

in which $q_n = 2\pi n/L$, all wavelength components $\hat{h}_{q_n}(t)$ with a wavenumber $q_n \geq \pi/\ell$ were set to zero. For $\Delta h_i(t)/\tau$ we used the forward difference approximation with $\Delta h_i(t) = h_i(t+\tau) - h_i(t)$. Subsequent differentiations and multiplications were carried out in the Fourier and the real space, respectively. The parameter vector $\mathbf{a}$ was then determined by solving $\min_{\mathbf{a}} \mathcal{J}(\mathbf{a})$, where

$$\mathcal{J}(\mathbf{a}) = \left\langle \left[\frac{\Delta h_i(t)}{\tau} - \mathbf{a}\cdot\mathbf{H}_i(t) \right]^2 \right\rangle_{i,t} . \tag{7}$$

Notice that in equation (7) it is implicitly assumed that the noise characteristics, distributions and correlations of $\eta_i(t)$, are the same for all the data over which the average is taken. Moreover, basically one should also include in equation (7) the restriction of the relevant coefficients into physically reasonable values (*e.g.* c and ν should be positive). Here, however, the relevance of the values obtained was checked only afterwards. Once a minimizer $\mathbf{a}^*$ of equation (7) is determined, the noise correlator D follows from

$$D = \frac{\ell\tau}{2}\,\mathcal{J}(\mathbf{a}^*)\ . \tag{8}$$

All the parameters c, ν, λ, and D thus obtained depend on the spatial and temporal resolution ℓ and τ, respectively. For c and λ we however expect to find convergence to constant values independent of coarse graining for large enough values of ℓ and τ, while no such convergence is expected for ν and D [15].

3.2 Results

In Figure 1 (Fig. 2) we show the averaged KPZ coefficients c, λ, ν, and D for the copier-paper (lens-paper) burns as functions of the spatial coarse-graining parameter ℓ, for different values of the temporal coarse-graining parameter τ. For small τ when the effects of temporal discretization vanish more rapidly, coefficients c and λ level off at relatively small ℓ to more or less constant values. For larger τ leveling off appears at larger ℓ, but the asymptotic values of the parameters seem to be quite close to the plateaux found for small τ. We therefore found it sensible to determine the parameter values for a small coarse-graining time, $\tau = 0.4$ s, as averages over a fairly short length scale just above the crossover scale (to the asymptotic KPZ behavior) in the spatial height-height correlation function: $\ell \in [11.6\text{ mm}, 17.6\text{ mm}]$. Coarse-graining time was now smaller than the crossover time, and the results obtained should be somewhat affected by the correlated non-Gaussian noise at short time scales [8],

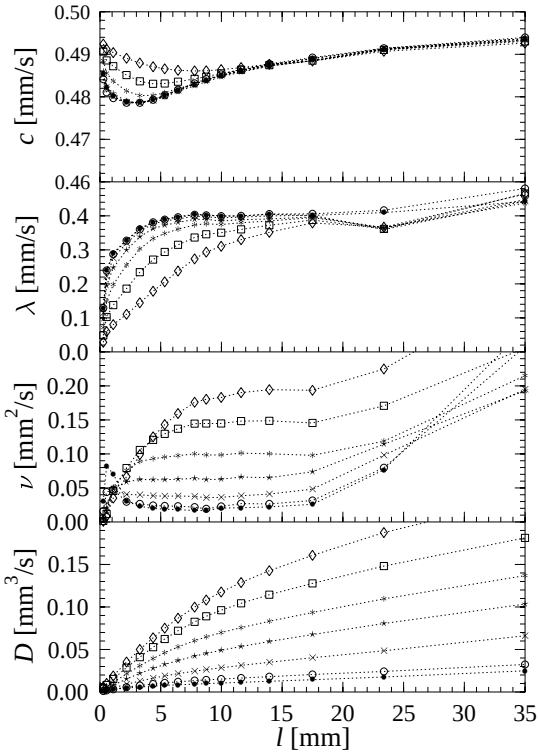

Fig. 1. Coarse graining of the model parameters c, λ, ν, D determined by the inverse method and averaged over 18 copier-paper burns. Here ℓ is the cutoff wavelength of the Fourier components and the values of τ are 0.4 ($\cdot$), 0.8 ($\circ$), 1.6 ($\times$), 3.2 ($\star$), 6.4 ($*$), 12.8 ($\square$), and 25.6 s ($\diamond$).

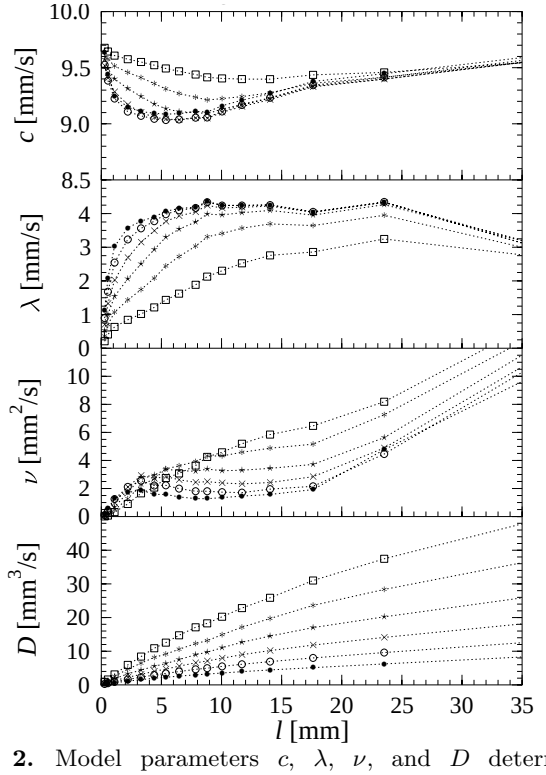

Fig. 2. Model parameters c, λ, ν, and D determined by the inverse method and averaged over 32 lens-paper burns, as functions of the cutoff length ℓ for τ = 0.1 ($\cdot$), 0.2 ($\circ$), 0.4 ($\times$), 0.8 ($\star$), 1.6 ($*$), and 3.2 s ($\square$).

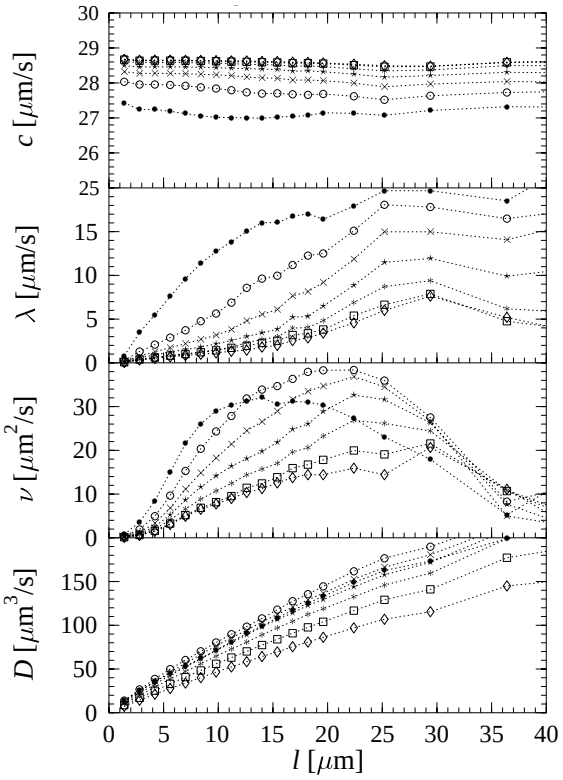

Fig. 3. Model parameters c, λ, ν, and D determined by the inverse method and averaged over 9 sets of magnetic flux fronts, as functions of the cutoff length ℓ for τ = 0.5 ($\cdot$), 1.0 ($\circ$), 1.5 ($\times$), 2.0 ($\star$), 2.5 ($*$), 3.0 s ($\Box$), and 3.5 ($\diamond$) s.

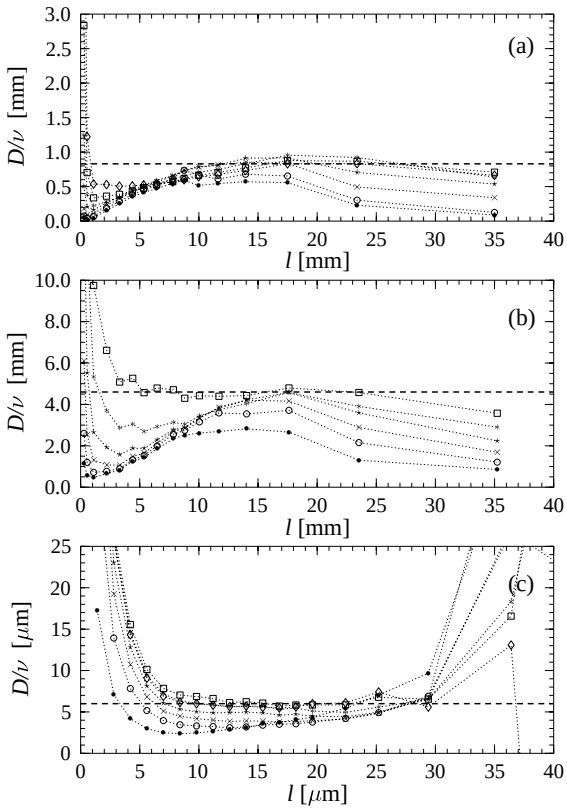

Fig. 4. The renormalization of the ratio D/ν as a function of the cutoff length ℓ for (a) copier-paper and (b) lens-paper fronts, and (c) magnetic flux fronts. For each case the symbols for different τ's corresponds to those used in Figures 1–3, respectively.

as the inverse method assumes uncorrelated white noise. This effect seems however to be quite small. We find that $c = 0.49(2)$ mm/s and $\lambda = 0.40(2)$ mm/s for the copier-paper fronts, and $c = 9.2(5)$ mm/s and $\lambda = 4.1(2)$ mm/s for the lens-paper fronts.

Figure 3 shows the averaged KPZ coefficients as functions of ℓ for the magnetic flux fronts. The values were obtained by averaging over 9 sets of fronts measured on the same sample. The inverse method and the system size set an upper limit for the feasible coarse-graining length, $\ell \approx 45$ μm, for the current sets of fronts, which is somewhat smaller than the crossover length $r_c \approx 60$ μm estimated from the spatial height-height correlation function in reference [9]. Estimates for coefficients c and λ were now made as averages over the coarse-graining lengths $\ell \in$ [11.2 μm, 19.6 μm], and, by similar reasoning as above, for $\tau = 0.5$ s. Since all nine measurements were made on the same sample, noise averaging (over structural defects in the sample) was less extensive than for the slow-combustion fronts, and saturation of the parameter values was not quite as good. c and λ can however be measured by other methods, and we think the values found by the inverse method, $c = 27.0(1)$ μm/s and $\lambda = 15.9(8)$ μm/s, are fairly reliable as they are consistent with the other estimates.

Because of a fluctuation-dissipation theorem, coefficients ν and D are expected [10] to depend asymptotically in the same way on the coarse-graining parameter ℓ (see below and [15] on the effects of finite τ) so that their ratio should converge to a constant value. We therefore show in Figure 4 the ratio of noise correlator D to 'surface tension' ν for the fronts in both paper grades and the magnetic flux fronts. Asymptotically this ratio indeed seems to converge to a constant value for all cases. This asymptotic value appears to approach the one D/ν reaches, for larger coarse-graining times, toward the upper ends of the length intervals used to determine the estimates for c and λ, so we determined this ratio for $\ell = 17.5$ mm and $\tau = 25.6$ s for the copier-paper fronts, $\ell = 17.6$ mm and $\tau = 1.6$ s for the lens-paper fronts, and $\ell = 19.6$ μm and $\tau = 3.5$ s for the magnetic flux fronts.

In this way we find that D/ν is 4.6(1.1) mm for the lens-paper fronts, 0.83(5) mm for the copier-paper fronts, and 6(3) μm for the magnetic flux fronts. Previously, we have reported [8] values for the asymptotic amplitude A of the spatial height-height correlation function, which is $A = D/\nu$. The reported results, $D/\nu \simeq 3.4$ mm for the lens-paper and $D/\nu \simeq 0.48$ mm for the copier-paper fronts, are in fairly good agreement with the present results, especially with those for lens paper, which have the best statistics.

Assigning individual values to ν and D is not straightforward as they admit renormalization. Simulation results

Table 1. Measured average values for KPZ coefficients and the ratio D/ν. For the slow-combustion fronts $l = 11.6 \ldots 17.6$ mm and $\tau = 0.4$ s, and for the magnetic flux fronts $l = 11.2 \ldots 19.6$ μm and $\tau = 0.5$ s, were used as the coarse-graining scales for c and λ. The scaled ν and the D/ν ratio were determined for $\ell = 17.5$ mm and $\tau = 25.6$ s (copier-paper), and $\ell = 17.6$ mm and $\tau = 1.6$ s (lens-paper). The D/ν ratio for the magnetic flux was determined for $\tau = 3.5$ s and $\ell = 22.4$ μm.

Coefficient	Inverse method			Slope-dependent velocity		
	Copier $\times 1$	Lens $\times 1$	Flux $\times 10^{-3}$	Copier $\times 1$	Lens $\times 1$	Flux $\times 10^{-3}$
c [mm/s]	0.49(2)	9.2(5)	27.0(1)	0.485(2)	9.1(2)	27.1(2)
λ [mm/s]	0.40(2)	4.1(2)	15.9(8)	0.37(3)	5.1(2)	17.4(2)
$\nu \left(\frac{\tau}{\Delta t}\right)^{-1/3}$ [mm^2/s]	0.049(3)	2.0(1)	–	–	–	–
$D\nu$ [mm]	0.83(5)	4.6(1.1)	6(3)	–	–	–

indicate [15] that for finite τ they should level off as functions of ℓ to values that scale as τ^β. For totally uncorrelated fronts this is also expected from renormalization-group flows for the KPZ equation (in 1+1 dimensions) [15] as then renormalization at large ℓ is controlled by τ. For ν this appears to be the case for the slow-combustion fronts, for intermediate values of ℓ. Asymptotically (in ℓ) there is however indication that ν scales roughly as ℓ^χ, but continues to have a similar τ-dependent amplitude. For the magnetic flux fronts tendency is rather similar but, probably due to averaging being too limited for this particular quantity, there is not enough accuracy to determine the actual scaling. Therefore, we show in Table 1 the scaling form $\nu(\tau/\Delta t)^{-\beta}$ only for the slow-combustion fronts. Here the same coarse-graining parameters were used as for the D/ν ratio. For increasing τ discreteness effects begin to appear at small ℓ, and possible leveling off of the $\nu(\ell)$ curves appears at larger values of ℓ. In the case of slow-combustion fronts, effective noise also plays a role at small ℓ's. In the case of magnetic flux fronts the structure of effective noise is different. There is rather little structural disorder in the samples in small length scales, and it mainly appears in (relatively speaking) large scales. This is the probable reason for the 'reverse' τ dependence of both ν and D in the slow-combustion and magnetic flux fronts.

For D no τ-dependent leveling off was observed for any data. Especially for increasing τ values D seems to behave roughly as $\tau^\beta \ell^\chi$, but we do not have any argument to support this kind of behavior, and give here no scaling forms for D. In Table 1 we have thus listed the averaged experimental values for c, λ, $\nu(\tau/\Delta t)^{-\beta}$, and D/ν, as determined for the coarse-scaling scales specified above. It is of course possible that leveling off would appear at still higher values of ℓ. However, for the present widths of the samples the statistics for increasing ℓ become too low to actually observe it.

We also tested the inverse method for non-KPZ equations by including higher-order terms with related coefficients, and comparing the results with those from numerical simulations of a discretized KPZ equation with real noise as determined by optical scans of lens-paper samples. It appears that the inverse method finds it difficult to distinguish, *e.g.*, a fourth-order derivative from noise, while the other KPZ parameters seemed to be more or less unaffected by inclusion of this term. On the other hand, the data produced by KPZ simulations with real noise gave as well rise to a non-zero fourth-order derivative when the inverse method was applied to these data. Also, the coefficient of the fourth-order derivative was higher for the simulated data than for the measured data. In this sense we can conclude that no evidence was found for the existence of higher-order terms in the equation of motion for the measured fronts. Evidently, a more robust inverse method should be used to determine the actual form of the evolution equation from noisy experimental data, if possible at all.

4 Slope-dependent velocity

4.1 Theory

An alternative way to measure c and λ from experimental data can be based on the fact that front velocity, in the length scale being considered, depends on the average slope of the front in that scale. For a front whose dynamics is governed by the KPZ equation, equation (1), the average velocity v in scale ℓ is given by

$$v = v_0 + \frac{\lambda}{\ell} \int_0^\ell \mathrm{d}\mathbf{x} \, \sqrt{1 + (\nabla h)^2}, \tag{9}$$

where v_0 is the drift velocity due to the external forces acting on the front, and we have kept the full square-root term in this expression. Assuming $(\nabla h)^2$ is small, the above expression can be expanded as usual so that

$$v \approx v_0 + \frac{\lambda}{\ell} \int_0^\ell \mathrm{d}\mathbf{x} \, \left[1 + \frac{1}{2}(\nabla h)^2 - \frac{1}{8}(\nabla h)^4 + \ldots \right] \tag{10}$$

$$= c + \frac{\lambda}{2\ell} \int_0^\ell \mathrm{d}\mathbf{x} \, (\nabla h)^2 + \mathcal{O}\left[(\nabla h)^4\right] , \tag{11}$$

where $c \equiv v_0 + \lambda$ is the zero-slope velocity.

If there is now a non-zero average slope $m \equiv \langle (\nabla h) \rangle$ in an interval of length ℓ of the front, the result equation (11) means that the front velocity in that interval is given by

$$v(m) \approx c + \frac{\lambda}{2} m^2. \tag{12}$$

The $v(m)$ of equation (12) is the local-slope dependent velocity as observed in a coarse-grained scale ℓ. By measuring $v(m)$, one should thus find a parabolic dependence which, by equation (12), gives an estimate for the coefficient of the nonlinear term, λ [2,3].

From experimental data the slope-dependent front velocity can be evaluated by applying, *e.g.*, the procedure described by Albert *et al.* [14]: the discretized front height $h_i(t)$ of length N $(= L/\Delta x)$ is partitioned into overlapping segments of length ℓ. The local slope $s_i(t)$ of each segment i at time t is determined by a linear fit to the interval $(i, i+\ell-1)$, with $i = 1, 2, \ldots, (N-\ell+1)$. The same partitioning, and determination of the slopes of the segments, is then repeated for the front at time $t+\tau$, and the average velocity of each segment (local velocity) is determined from

$$u_i(t) = \frac{1}{\ell} \sum_{j=0}^{\ell-1} \left[\frac{h_{i+j}(t+\tau) - h_{i+j}(t)}{\tau} \right] . \qquad (13)$$

The average velocity of all segments with slope s is then given by

$$u(s) = \frac{1}{N(s)} \sum_{i,t} u_i(t) \ , \qquad (14)$$

where $s_i(t) \in [s - \Delta s/2, s + \Delta s/2]$ with Δs a suitable discretization step for the slope values, and $N(s)$ is the number of such segments. The slope of each segment is determined as the average of the initial (at time t) and final (at time $t + \tau$) slope. In the following we will use the values $\Delta s = 4 \times 10^{-3}$ for both paper grades, and 0.1 for the magnetic flux fronts. If $u(s)$ plotted as a function of s indeed has a parabolic form, it indicates that a slope-dependent nonlinear term is present in the growth equation.

4.2 Results

We determined the local-slope dependent velocity $u(s)$ for the two sets of smouldering paper data and the magnetic flux front data described above. Figures 5–7 show the slope-dependent velocities for the copier-paper, lens-paper, and magnetic flux fronts, as functions of s^2, for several τ's and ℓ's. In all three sets of results, a linear trend was found in the $u(s)$ *vs.* s^2 curve, for all τ's and ℓ's, when $s \to 0$. This linear behavior broke down with increasing s for small segment lengths ℓ (see Figs. 5a and 6a), which could be explained by adding higher order terms in the expansion equation (11). However, the effect of higher-order terms vanished for increasing coarse graining, *i.e.*, when the segment length ℓ was increased. We found that the zero-slope velocities were $c = 0.49(2)$ mm/s and $c = 9.1(2)$ mm/s for the copier-paper and lens-paper fronts, respectively, and $c = 27.1(5)$ μm/s for the magnetic flux fronts.

We estimated the dependence of front velocity on higher-order terms by fitting the $u(s)$ curves by nth degree polynomials (for even n)

$$p_n(s) = a_n s^n + a_{n-1} s^{n-2} + \cdots + a_2 s^2 + a_0 \ ,$$

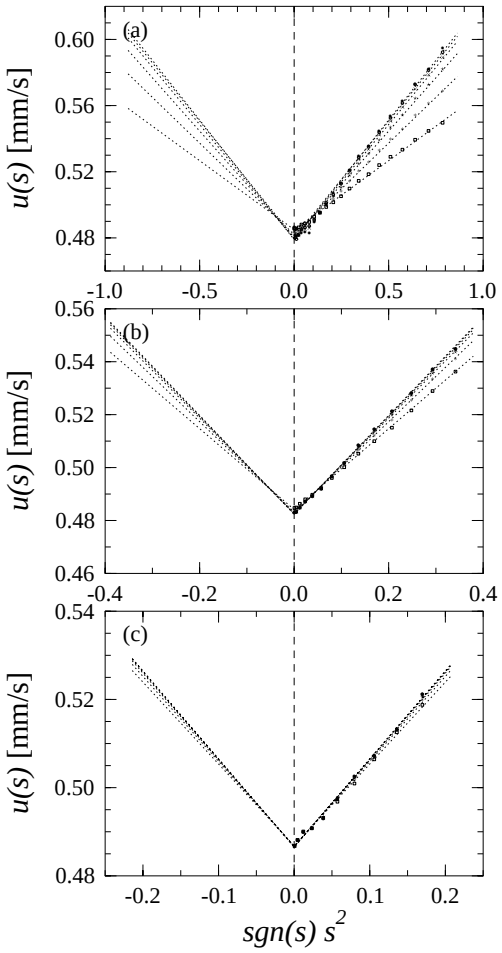

Fig. 5. Determination of λ from the slope-dependent velocity of the interface. The average velocity of segments of copier-paper fronts are shown as a function of s^2, with s the slope of the segment, for $\tau = 0.4,\ 0.8,\ 1.6,\ 3.2,\ 6.4$, and 12.8 s (from top to bottom). The plots (a)-(c) are for segment lengths 1.1, 8.7, and 17.5 mm, respectively.

where n was chosen so as to produce an optimal *reduced* χ^2-value. Before these fits the measured velocities were symmetrized ($u(-s) = u(s)$ for fronts that are governed by KPZ dynamics) by replacing $u(s)$ by

$$u(s) \equiv \frac{N(-s)u(-s) + N(s)u(s)}{N(-s) + N(s)} . \qquad (15)$$

The polynomial fits were then done in the region $[0, s']$ with $n = 2$ (copier-paper and flux-front results) and $n = 6$ (lens-paper results). From these fits we found that $\lambda = 0.37(3)$ mm/s and $\lambda = 5.1(2)$ mm/s for the copier-paper and lens-paper fronts, respectively, and $\lambda = 17.4(2)$ μm/s for the magnetic flux fronts. With $f(s) = N(s)/\sum_{s'} N(s)$ the slope-frequency distribution, the fitting region $[0, s']$ was defined so that $\int_0^{|s'|} f(s)\,\mathrm{d}s \approx 0.99$. It also became evident from our fits for the lens-paper fronts that the ratio of the fourth-order and second-order terms approached that of the square-root expansion in equation (10) when $\ell \to 0$ (estimated ratio $a_4/a_2 = -0.25(3)$ for $\ell \simeq 1.1$ mm,

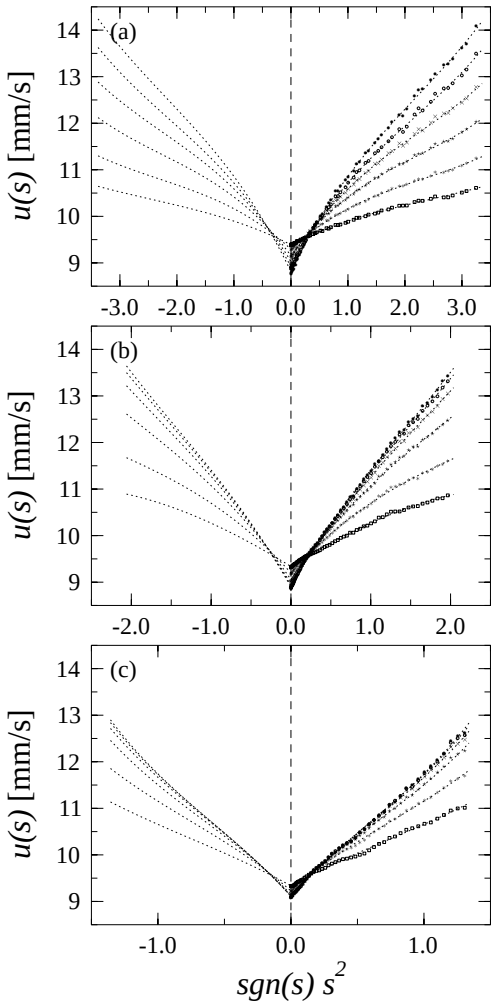

Fig. 6. The average velocity of segments of lens-paper fronts as a function of s^2, with s the slope of the segment, for $\tau =$ 0.2, 0.4, 0.8, 1.6, 3.2 and 6.4 s (from top to bottom). The plots (a)-(c) are for segment lengths 1.1, 8.8, and 17.6 mm, respectively.

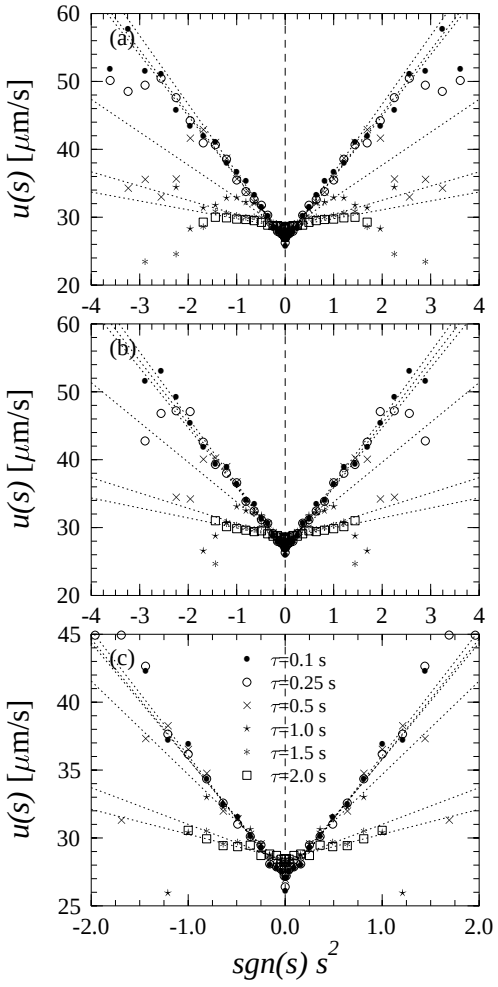

Fig. 7. The average velocity of segments of magnetic flux fronts as a function of s^2, with s the slope of the segment, for $\tau = 0.1,\ 0.25,\ 0.5,\ 1.0,\ 1.5$ and 2.0 s (from top to bottom). The plots (a)-(c) are for segment lengths 8.4, 14.0, and 19.6 μm, respectively.

cf. Fig. 8). Including higher-order terms in the fits to the $u(s)$ curves gave more accurate estimates for coefficient λ.

5 Discussion

In summary, we have determined the effective coefficients of the KPZ equation for experimental data on slow-combustion fronts in two grades of paper, and on magnetic flux fronts in a high-T_c thin-film superconductor, using partly two methods. For two of the coefficients, *i.e.*, the zero-slope velocity c and the nonlinear term λ, both these methods could be used, and the resulting estimates were in good agreement with each others. In fact three methods can be used to determine c as it can also be estimated from the time evolution of the average front height. We also obtained estimates for the ratio D/ν of the noise correlator D and the 'surface tension' ν by using

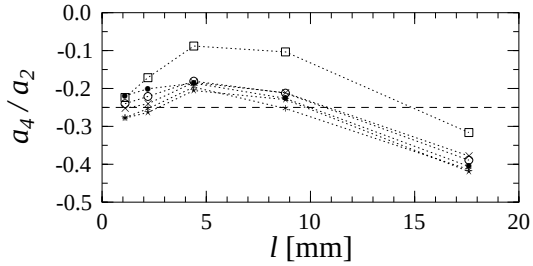

Fig. 8. Ratio a_4/a_2 as a function of segment length ℓ for all used τ values of the lens-paper data to test the expansion $\sqrt{1+(\nabla h)^2} \approx 1 + \frac{1}{2}(\nabla h)^2 - \frac{1}{8}(\nabla h)^4$.

the inverse method. For slow-combustion fronts the D/ν thus obtained could be compared with a previous result [8] for the asymptotic amplitude of the spatial height-height correlation function, $A = D/\nu$, with again good agreement. In all cases this ratio was found to converge quite well for increasing coarse-graining scales ℓ and τ. For ν

a τ-dependent scaling form was determined for the slow-combustion fronts.

The parabolic dependence of the local front velocity on the local slope of the front provides fairly direct independent evidence of the existence of a KPZ type nonlinear term in the evolution equation. Furthermore, higher-order polynomial fits to the slope-dependent front velocity of the lens-paper fronts lend some support to a square-root form of the slope dependence, expected when driving is along the local normal. This shows up at short length scales, asymptotically the higher-order terms are irrelevant.

For slow-combustion fronts saturation as a function of the coarse-graining length of the parameters appears to be so rapid that short coarse-graining times could be used to determine c and λ. For magnetic flux fronts saturation is slower, but comparison of results of different methods indicates that even then short coarse-graining times can rather reliably be used. For these latter fronts noise averaging was not extensive as all fronts were measured on only one sample. The overall coarse-graining behaviors of all fronts were fairly similar, and to a large extent understandable from the general structures of the fronts. The difference in the nature of noise between the paper samples and the thin-film superconductor used, is expected to explain the 'reverse' τ dependence in these two cases.

The inverse method used here does not seem to be sensitive enough to handle higher-order derivatives in the evolution equation for real experimental systems, it cannot properly distinguish these terms from noise. This may of course be due to decreasing statistics in the data for increasing coarse-graining length. This method cannot thus be reliably used to infer the detailed form of the evolution equation from noisy experimental data, beyond the leading-order terms. For these leading terms the method seems however to provide fairly reliable estimates. Comparison with simulation results indicates, however, that higher-order terms are not relevant for slow-combustion fronts in lens paper, which were used as a test case as they had the best statistics. As the behavior of all experimental fronts was qualitatively very similar, we expect the same to hold for the other systems as well.

Increasing the spatial resolution in the imaging of the fronts would not improve the inversion method results, as the important question is how the model parameters behave asymptotically as functions of the coarse-graining length. A real limitation is that only $\ell \leq L/4$ are meaningful length scales in the analysis. A significant improvement here does not seem possible for practical reasons. Improving the statistics would obviously make the estimates more reliable. On the other hand, the more sophisticated inversion method by Giacometti and Rossi [17] could not be used for our experimental data at all, because the most prominent evolution of the relevant correlation functions occurred within a too short (with our experimental time resolution and statistics) time window.

It may well be that more robust inversion methods should be developed for analyzing experimental data. The new robust filtering method used here to remove accidental defects from the recorded front lines was efficient, and made a noticeable improvement in the quality of the results. A similar approach, which can be used as a basis for inversion problems (*cf. e.g.* Ref. [19]), can also be used in combination with different computational techniques [20].

Appendix A: Robust methods in filtering

For digital images that contain noise and other degradations due to non-Gaussian distributions and outliers, so-called robust methods must be applied for proper restoration of the true image (see, *e.g.*, [21,22] and references therein). The basic principle behind such methods is simple: whereas the discrete, univariate sample mean

$$\min_{\mu_2} \sum_{i=1}^{N} |\mu_2 - x_i|^2,$$

i.e., $\sum_{i=1}^{N}(\mu_2^* - x_i) = 0$, is sensitive to the actual distance between the estimator and the given data, the corresponding median $\min_{\mu_1} \sum_{i=1}^{N} |\mu_1 - x_i|$, *i.e.*, $\sum_{i=1}^{N} \mathrm{sign}(\mu_1^* - x_i) = 0$, is not.

The most commonly used robust image restoration method is the so-called median filter which uses an *a priori* chosen or adaptively determined window for locating the seek of the median value [23]. Although this procedure is robust for single outliers, the median filter does not contain any control of the smoothness of the restored image. This is why the obtained result typically has a staircase- or rump-like structure for small windows, and becomes more and more blurred when the window size increases.

We describe below in a continuous setting the main ideas of the restoration scheme applied here. The restored image $u(x,t)$ is obtained as the solution of the optimization problem

$$\min_{u} \mathcal{J}(u) \tag{16}$$

with

$$\mathcal{J}(u) = \int_{\Omega} \left[|u - z| + \frac{\beta_1}{2} \left| \frac{\partial u}{\partial x} \right|^2 + \frac{\beta_2}{2} \left| \frac{\partial u}{\partial t} \right|^2 \right] \mathrm{d}x\, \mathrm{d}t, \tag{17}$$

in which z represents the experimental data. The cost functional to be minimized, equation (17), consists of two parts. The first part introduces a robust and outlier-insensitive fitting in L^1 norm between the solution and the noisy observation. The second part controls the regularity of the solution in an orthotropic manner, and allows to impose different behaviors in the x and t directions. For $\beta_1, \beta_2 > 0$, $\mathcal{J}(u)$ is strictly convex, so that equation (16) admits a unique solution u^* [24]. However, due to the L^1 term $\mathcal{J}(u)$ is nondifferentiable in the classical sense (derivative of $|x|$ is multivalued at $x = 0$) so that ordinary optimization methods like the steepest-descents or the conjugate-gradient method cannot be applied for solving equation (16) [25,26].

The actual discrete counterpart of equations (16–17) can be expressed in the form

$$\min_{u \in \mathbb{R}^N} J(u) \tag{18}$$

with

$$J(u) = |M(u-z)|_1 + \frac{\beta_1}{2} u^T K_x u + \frac{\beta_2}{2} u^T K_y u. \quad (19)$$

Here, $|v|_1 = \sum_i |v_i|$ denotes the discrete l_1 norm, v^T the transpose of vector v, K_x and K_y directional stiffness matrices, and M the diagonal lumped mass matrix of FEM discretization of equation (17) [27]. A heuristic interpretation of equations (18–19) is that locally a median-like value is restored, and global smoothness is assured, by the orthotropic regularization that defines a norm which is equivalent to the (discrete) H^1 norm. The shape of the local neighborhood and the strongness of the fitting are both determined by the chosen values of parameters β_1 and β_2.

In practice, we first apply a technique similar to that of equations (18–19) on the (1D) boundary of the experimental data. These presmoothed values at the boundaries are then used as a nonhomogeneous boundary condition in equation (18). The actual algorithm for the robust restoration of a given image z is the following.

0° **Initialization:** Choose $\beta_1, \beta_2 > 0$.

1° **Boundary fix:** Let $\tilde{M}$ and $\tilde{K}$ denote the 1D FE mass and stiffness matrix, respectively. Solve the 1D restoration problem

$$\min_{\tilde{u}} |\tilde{M}(\tilde{u}-z)|_1 + \tilde{\beta}\tilde{u}^T \tilde{K}\,\tilde{u}$$

separately on the boundary strips $\Gamma_1 = (x_0, x_1) \times y_0$, $\Gamma_2 = (x_0, x_1) \times y_1$, $\Gamma_3 = x_0 \times (y_0, y_1)$, and $\Gamma_4 = x_1 \times (y_0, y_1)$, by using stronger smoothing: $\tilde{\beta} = 30\,\beta_1$ on $\Gamma_1 \cup \Gamma_2$ and $\tilde{\beta} = 30\,\beta_2$ on $\Gamma_3 \cup \Gamma_4$ (30 is a heuristic constant determined by test runs), with the observed values $\{z(x_0, y_0), z(x_1, y_0)\}$, $\{z(x_0, y_1), z(x_1, y_1)\}$, $\{z(x_0, y_0), z(x_0, y_1)\}$, and $\{z(x_1, y_0), z(x_1, y_1)\}$ on the corner points as the boundary conditions.

2° **Domain fix:** Solve the 2D restoration problem of equation (18) by using the obtained values from Step 1° as the nonhomogeneous boundary condition.

The full details of this methods are described in [28]. Figure 9 demonstrates the effect of filtering with $\beta_1 = \beta_2 = 0.01$ on the observed smouldering fronts in a lens-paper burn .

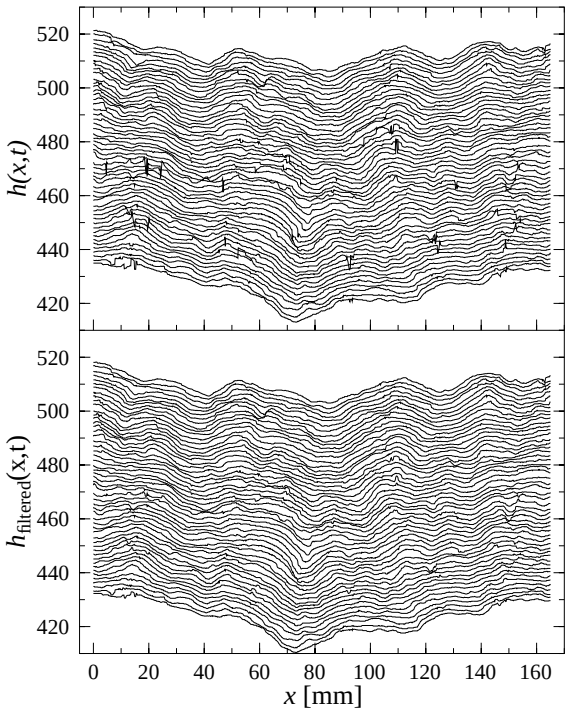

Fig. 9. Front profiles of a lens-paper burn before $[h(x,t)]$ and after $[h_{\mathrm{filtered}}(x,t)]$ filtering the data.

References

1. P. Meakin, Phys. Rep. **235**, 189 (1993)
2. T. Halpin-Healy, Y.-C. Zhang, Phys. Rep. **254**, 215 (1995)
3. A.-L. Barabási, H.E. Stanley, *Fractal Concepts in Surface Growth* (Cambridge University Press, Cambridge, UK, 1995)
4. P. Meakin, *Fractals, Scaling and Growth Far From Equilibrium* (Cambridge Universi Press, Cambridge, UK, 1998)
5. J. Zhang, Y.-C. Zhang, P. Alstrom, M.T. Levinsen, Physica A **189**, 383 (1992)
6. J. Maunuksela, M. Myllys, O.-P. Kähkönen, J. Timonen, N. Provatas, M.J. Alava, T. Ala-Nissila, Phys. Rev. Lett. **79**, 1515 (1997)
7. A.S. Balankin, D.M. Matamoros, Phil. Mag. Lett. **81**, 495 (2001)
8. M. Myllys, J. Maunuksela, M. Alava, T. Ala-Nissila, J. Merikoski, J. Timonen, Phys. Rev. E **64**, 036101 (2001), [cond-mat/0105234]
9. R. Surdeanu, R.J. Wijngaarden, E. Visser, J.M. Huijbregtse, J.H. Rector, B. Dam, R. Griessen, Phys. Rev. Lett. **83**, 2054 (1999)
10. M. Kardar, G. Parisi, Y.-C. Zhang, Phys. Rev. Lett. **56**, 889 (1986)
11. J. Krug, J. Phys. A **22**, L769 (1989)
12. L.A.N. Amaral, A.-L. Barabaási, H.E. Stanley, Phys. Rev. Lett. **73**, 62 (1994)
13. L.A.N. Amaral, A.-L. Barabási, H.A. Makse, H.E. Stanley, Phys. Rev. E **52**, 4087 (1995)
14. R. Albert, A.-L. Barabasi, N. Carle, A. Dougherty, Phys. Rev. Lett. **14**, 2926 (1998)
15. C.-H. Lam, L.M. Sander, Phys. Rev. Lett. **71**, 561 (1993)
16. A. Giacometti, M. Rossi, Phys. Rev. E **62**, 1716 (2000)
17. A. Giacometti, M. Rossi, Phys. Rev. E **63**, 046102 (2001)

18. R.J. Wijngaarden, K. Heeck, M. Welling, R. Limburg, M. Pannetier, K. van Zetten, V.L.G. Roorda, A.R. Voorwinden, Rev. Sci. Instrum. **72**, 2661 (2001)
19. J. Kaipio, V. Kolehmainen, E. Somersalo, M. Vauhkonen, Inverse Problems **16**, 1487 (2000)
20. T. Kärkkäinen, E. Heikkola, *Robust MLP*, no. C 1 in *Reports of the Department of Mathematical Information Technology. Series C. Software Engineering and Computational Intelligence* (Univeristy of Jyvaskyla, Finland, 2002)
21. C.R. Rao, Indian J. Statistics **50**, 289 (1988)
22. P.J. Huber, *Robust Statistics*, Wiley Series in Probability and Mathematical Statistics (John Wiley & Sons, New York, 1981)
23. R. Gonzalez, R. Woods, *Digital Image Processing* (Addison-Wesley, 1993)
24. I. Ekeland, R. Temam, *Convex Analysis and Variational Problems*, Vol. 1 of *Studies in Mathematics and its Applications* (North-Holland, Amsterdam, 1976)
25. M.M. Mäkelä, P. Neittaanmäki, *Nonsmooth Optimization. Analysis and Algorithms with Applications to Optimal Control* (World Scientific, Singapore, 1992)
26. J. Nocedal, S.J. Wright, *Numerical Optimization* (Springer, New York, 1999)
27. M. Krízek, P. Neittaanmäki, *Finite Element Approximation of Variational Problems and Applications*, Vol. 50 of *Pitman Monographs and Surveys in Pure and Applied Mathematics* (Longman Scientific & Technical, Essex, England, 1990)
28. R. Glowinski, T. Kärkkäinen, in preparation